Electronic Supplementary Information

A universal synthesis strategy for P-rich noble metal diphosphide based electrocatalyst for hydrogen evolution reactions

Zonghua Pu,[a] Jiahuan Zhao, [a] Ibrahim Saana Amiinu,[a] Wenqiang Li,[a] Min Wang,[a] Daping He,[a,b] and Shichun Mu[a,*]

[a] State Key Laboratory of Advanced Technology for Materials Synthesis and Processing, Wuhan University of Technology, Wuhan 430070, P. R. China

[b] Hubei Engineering Research Center of RF-Microwave Technology and Application, Wuhan University of Technology, Wuhan 430070, P. R. China.

* E-mail: msc@whut.edu.cn

1. Experimental Section

Materials: $IrCl_4 \cdot xH_2O$, $RhCl_3 \cdot 3H_2O$, $PdCl_2$ and melamine were purchased from Xinglong Chemical Corp. Ltd. KOH and H_2SO_4 were purchased from Beijing Chemical Works Ltd. Ethanol was purchased from Aladdin Reagents Ltd. Pt/C (20 wt%), Phytic acid (PA) and Nafion (5 wt%) were purchased from Sigma-Aldrich. All the reagents are analytical grade and used as received. De-ionized water was obtained from an ultra-pure purifier (Ulupure, China, resistivity ≥ 18.2 MΩ).

Preparation of IrP_2@NC: In a traditional way, 4.0 mL PA and 0.02 g $IrCl_4 \cdot xH_2O$ were dissolved in water by stirring, followed by addition of melamine. Then, the solution was dried at 80 ℃ 24 h to form a homogeneous powder. The solid mixture was transferred into a quartz tube and heated to 900 °C kept for 2 hours at a heating rate of 5 ℃ min^{-1} under N_2 atmosphere. The obtained products were washed by centrifugation with alcohol and water several times to remove the residue of reactants (Cl^- etc.), and finally dried in vacuum at 80 °C. Lastly, the samples of IrP_2@NC were obtained. For comparison, the NC and Ir@NC were also made.

Preparation the working electrode: 5.0 mg of the catalyst powder was dispersed in 980 μL ethanol/water (v/v=1:1) mixed solvents along with 20 μL 5 wt% of Nafion solution. Then the mixture was ultrasonically suspended for 30 min. After that 10 μL of this catalyst ink was dropped on the glassy carbon electrode (GCE: diameter = 3 mm) and dried at room temperature to obtain a catalyst loading of 0.7 mg cm^{-2}. The commercial catalyst ink was prepared by dispersing 10 mg catalyst in 1 mL mixed

solution of isopropyl alcohol and water (volume ratio 7:3) and 20 μL 5 wt% Nafon solutions. The mixed solutions were disposed for 15 min by ultrasonic cell disruptor, and then 5 μL homogeneous catalyst ink was deposited on the glassy carbon electrode, the electrode was allowed to dry at room temperature for 15 min to form a smooth catalyst ring. The catalyst loading for the commercial Pt/C (20 wt%) was 0.7 mg cm^{-2}. The Pt loading of Pt/C was about 0.14 mg cm^{-2}.

Material characterizations: Surface morphology was observed using JSM 7100F FESEM (Zeiss Ultra Plus) fitted with energy dispersive spectrum analyzer and operated at 5 kV. Structural features were characterized by transmission electron microscopy (TEM) on a JEM 2010 FEF microscope operated at 200 kV. Powder X-ray diffraction (XRD) patterns were collected on a Rigaku X-ray diffractometer equipped with a Cu Kα radiation source. X-ray photoelectron spectroscopy (XPS) spectra were recorded on a VG MultiLab 2000 spectrometer using Mg as the exciting source. Raman spectra were obtained on J-Y T64000 Raman spec-trometer with 514.5 nm wavelength incident laser light. Brunauer–Emmett–Teller (BET) specific surface area and pore size distribution measurement employed a Tristar 3020 gas adsorption analyzer at 77 K.

Electrochemical measurements: All electrochemical measurements are performed with a CHI 660D electrochemical analyzer (CH Instruments, Inc., Shanghai) in a standard three-electrode with two-compartment cell. Saturated calomel electrode (SCE) and Hg/HgO were used as reference electrode in 0.5 M H_2SO_4 and 1.0 M KOH,

respectively. A graphite rod (99.99%) was used as the counter electrode in all measurements. Polarization data were obtained at a scan rate of 5 mV s^{-1}. In all measurements, the reference electrode was calibrated with respect to reversible hydrogen electrode (RHE). All polarization curves were iR-corrected. Electrochemical impedance spectroscopy (EIS) measurements were carried out in the frequency range of 100 kHz–0.1 Hz with an AC amplitude of 10 mV. The iR-corrected potenetial was obtained after the correction of internal resistance measured by EIS following the equation:

$$E_{iR\text{-}corrected} = E - iR$$

where E is the original potential, R is the internal resistance, i is the corresponding current, and $E_{iR\text{-}corrected}$ is the iR-corrected potential.

2. Theoretical section

Computation details: The Plane-wave Density Functional Theory (DFT) calculations were conducted using the CASTEP module (an Ab Initio Total Energy Program) of Materials Studio 8.0 (Code version: 6546), with the hydrogen binding energy calculated from different active sites.[1,2] The generalized gradient approximation (GGA) method with a Perdew-Burke-Ernzerhof (PBE) functional was used to treat the electron exchange correlation (EEC) interaction.[3,4] The band energy and Fermi energy convergence tolerance were set at 1.0 $\times 10^{-5}$ and 2.7 $\times 10^{-5}$ eV, respectively. The DOS kpoint separation was set at 0.05 $Å^{-1}$. A Monkhorst–Pack grid k-points of 1×1×1 and a plane wave basis set cut-off energy of 300 eV were used for the

Brillouin zone integration. The structures were optimized for force and energy convergence set at 2.0×10^{-5} eV and 0.05 eV $Å^{-1}$, respectively. The self-consistence field (SCF) was 2.0×10^{-6} eV/atom. To consider the influence of van der Waals interaction, the semi-empirical DFT-D force-field approach was applied.[5,6] The Gibb's free energies for hydrogen absorption ΔG_{H*} were calculated from the given equation:

$$\Delta G_{H*} = \Delta E_{H*} + \Delta ZPE - T\Delta S$$

Where the symbols represent the binding energy (ΔE), the change in zero-point energy (ΔE_{ZPE}), Temperature (T), and the entropy change (ΔS) of the system, respectively. The $T\Delta S$ and ΔZPE are obtained as previously reported by Norskov et al. Thus, we adopted the approximation that the vibrational entropy of hydrogen in the adsorbed state is negligible, in which case $\Delta S_H \approx S_{H*} - 1/2(S_{H2}) \approx -1/2(S_{H2})$, where S_{H2} is the entropy of H_2(g) at standard conditions, and $TS(_{H2})$ is ~0.41 eV for H_2 at 300 K and 1 atm.[6]

Theoretical models: We have constructed the correlative theoretical models to simulate the sole NC, Ir/NC and composited IrP_2@NC nanomaterial. The pure or N-doped carbon layer is simulated by the single-layer carbon (C) or N-doped carbon (NC), respectively. The composite Ir_2P@NC model is constructed by covering the respective NC layer on the (200) facet of the IrP_2 slab. To minimize the lattice mismatch effects between the supported NC and the IrP_2 substrate, we have considered a surface (or interface) periodicity of 4×4 supercell for the NC, and 4×1 supercell for the IrP_2 in IrP_2@NC model, respectively.

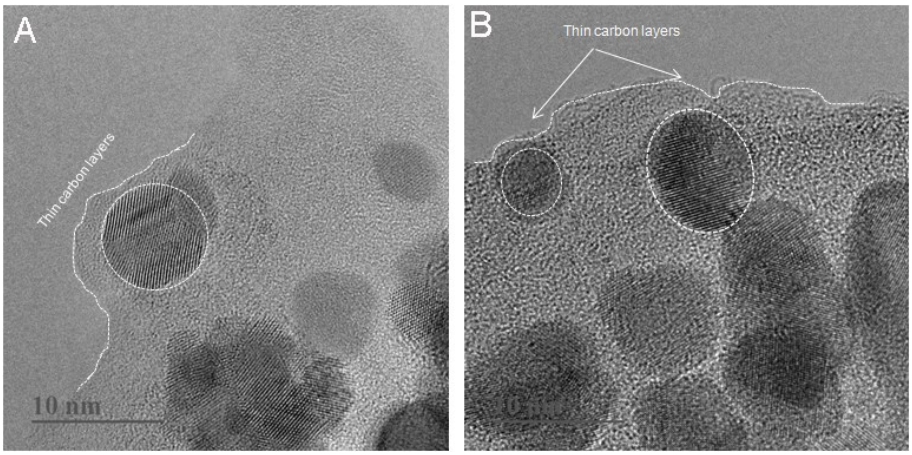

Fig. S1 HRTEM images of IrP_2@NC.

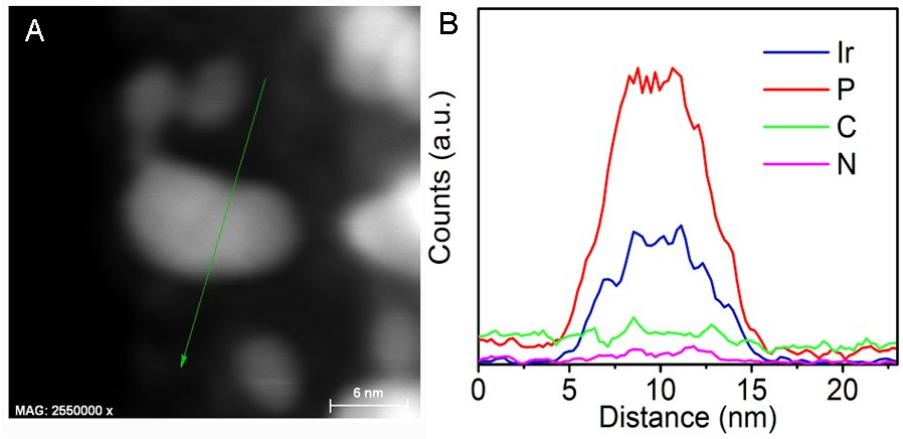

Fig. S2 (A) HAADF-STEM image of IrP_2@NC with the yellow line showing the line scanning path. (B) Corresponding line-scanning profile.

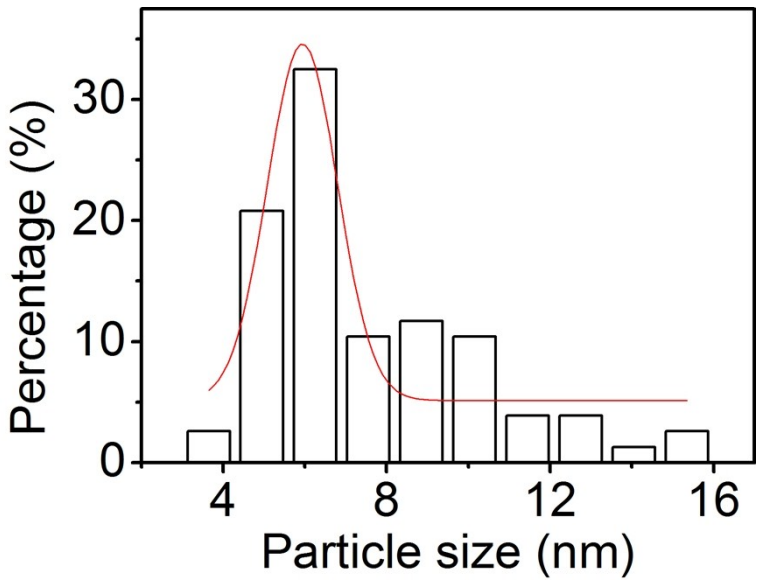

Fig. S3. Gaussian fitted size distribution of IrP_2 in IrP_2@NC.

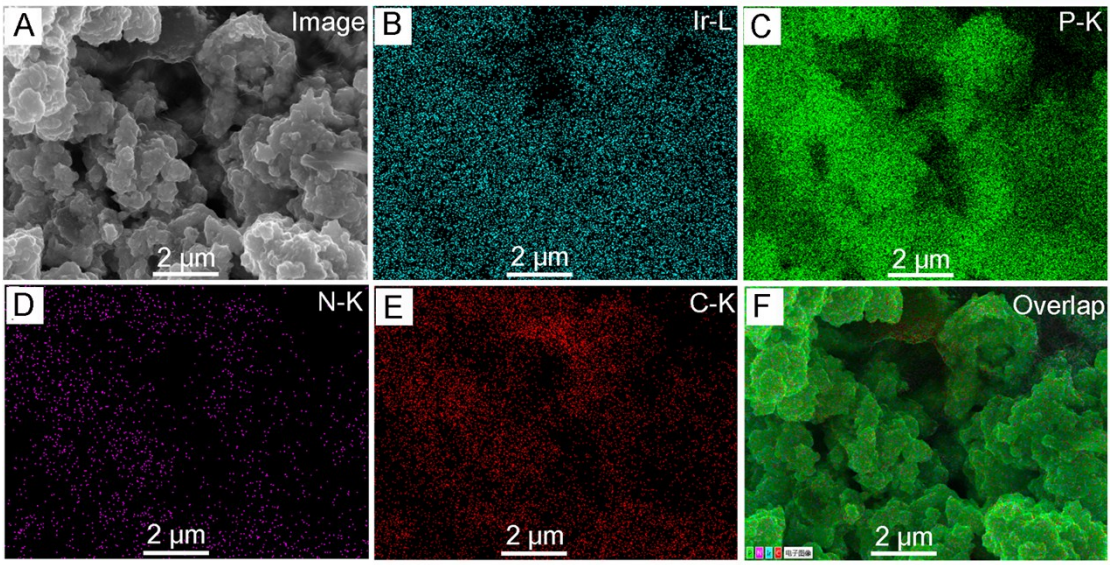

Fig. S4. (A-F) SEM image and EDX elemental mapping of Ir, P, N and C for IrP_2@NC.

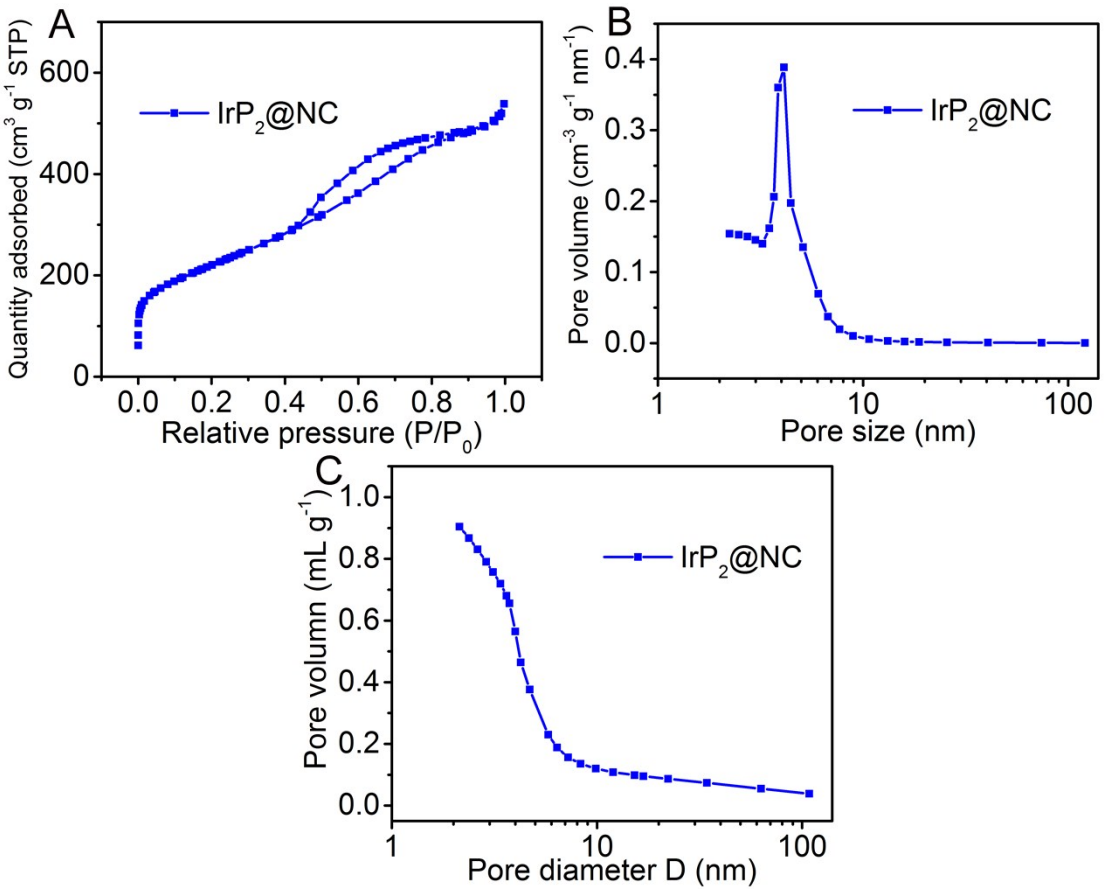

Fig. S5. (A) N_2 adsorption and desorption isotherms, (B) pore size distribution, and (C) pore volume of IrP_2/NC.

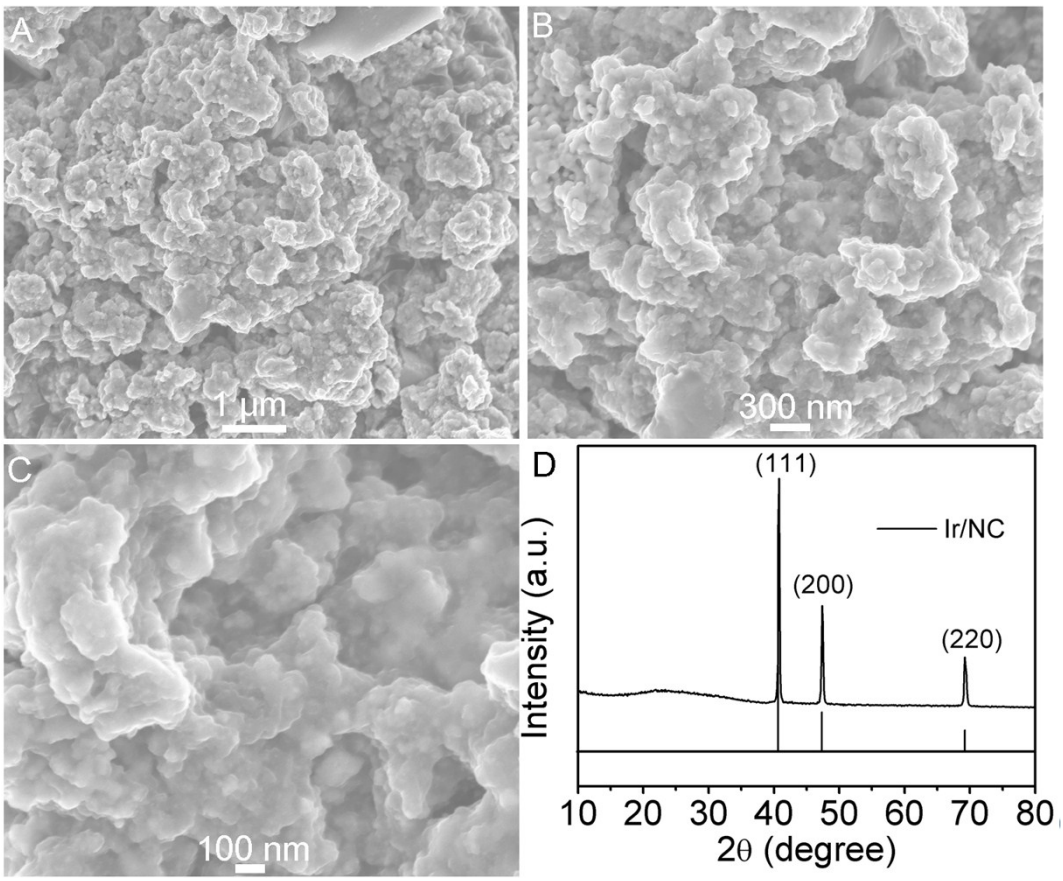

Fig. S6. (A-C) Low to high-magnification SEM images and (D) XRD pattern of Ir/NC.

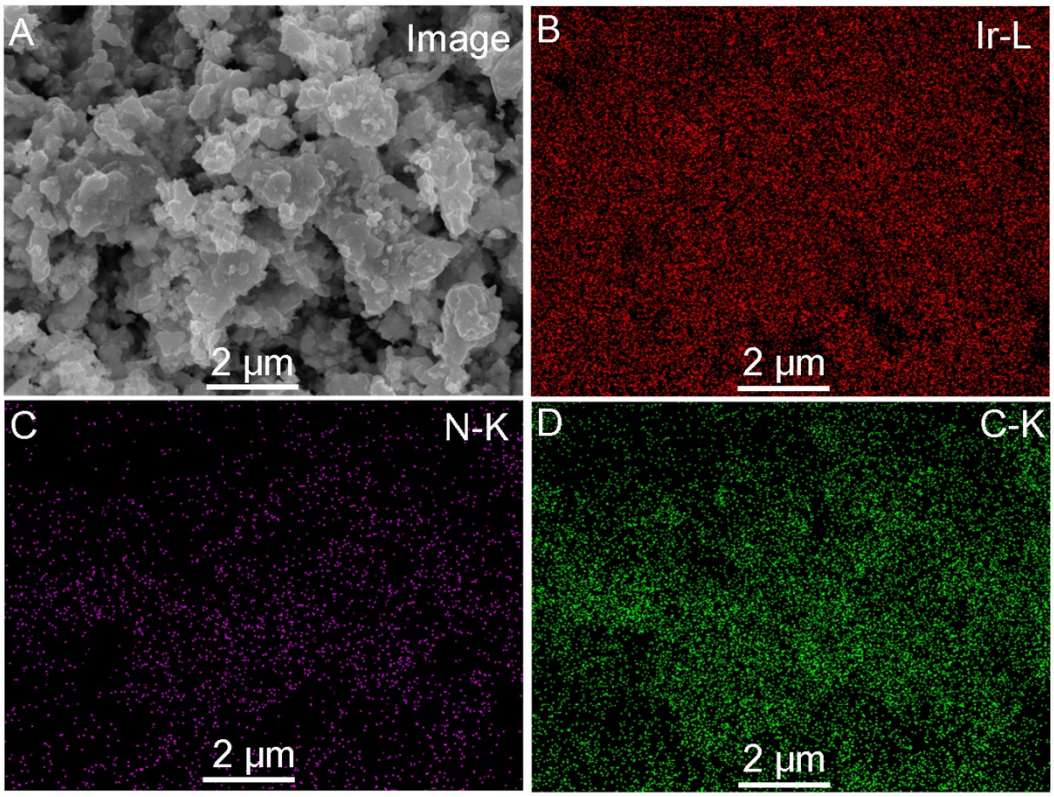

Fig. S7. (A) SEM image and (B-D) EDX elemental mapping of Ir, N and C for Ir/NC.

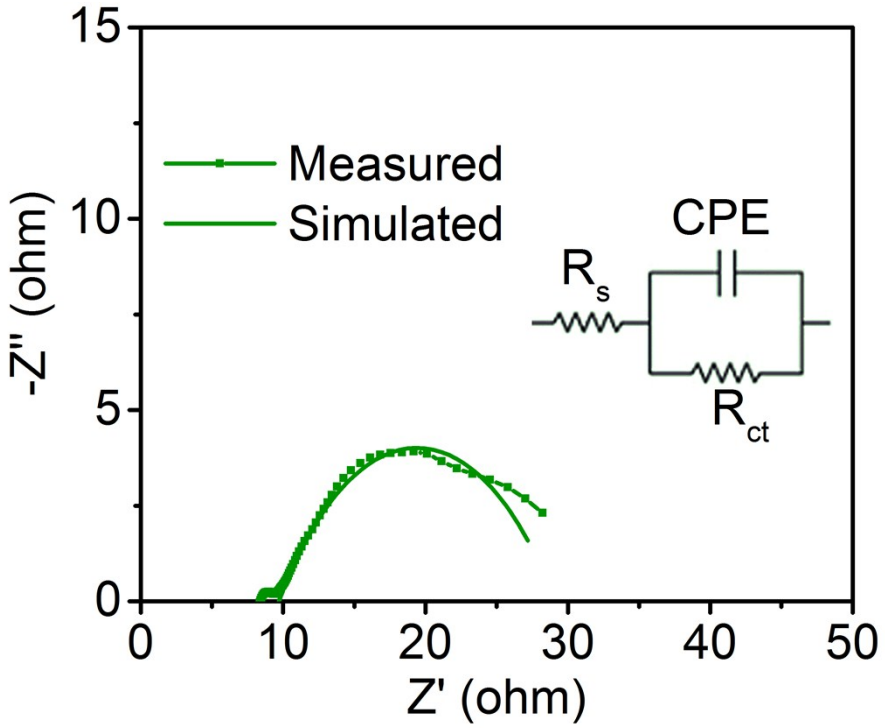

Fig. S8. Nyquist plots of IrP_2@NC recorded at 0 V vs. RHE in 0.5 M H_2SO_4.

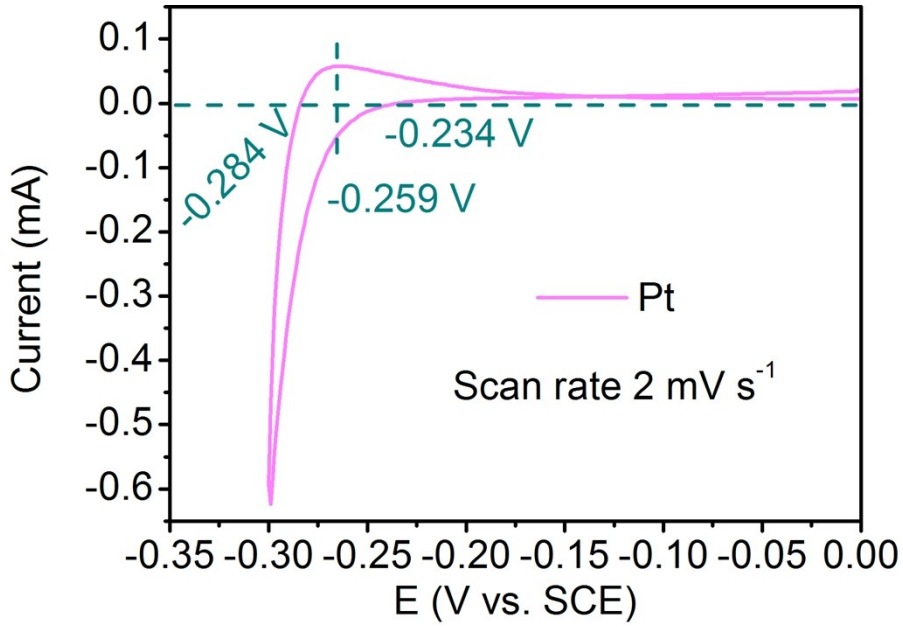

Fig. S9. RHE voltage calibration.

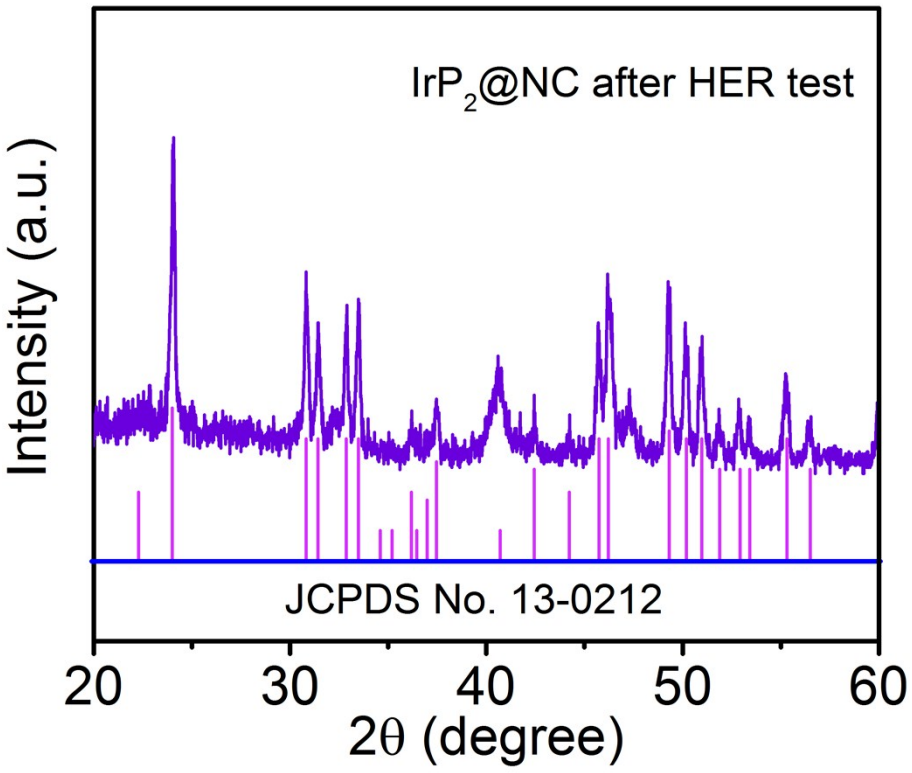

Fig. S10. XRD pattern of IrP_2@NC after long-term stability test.

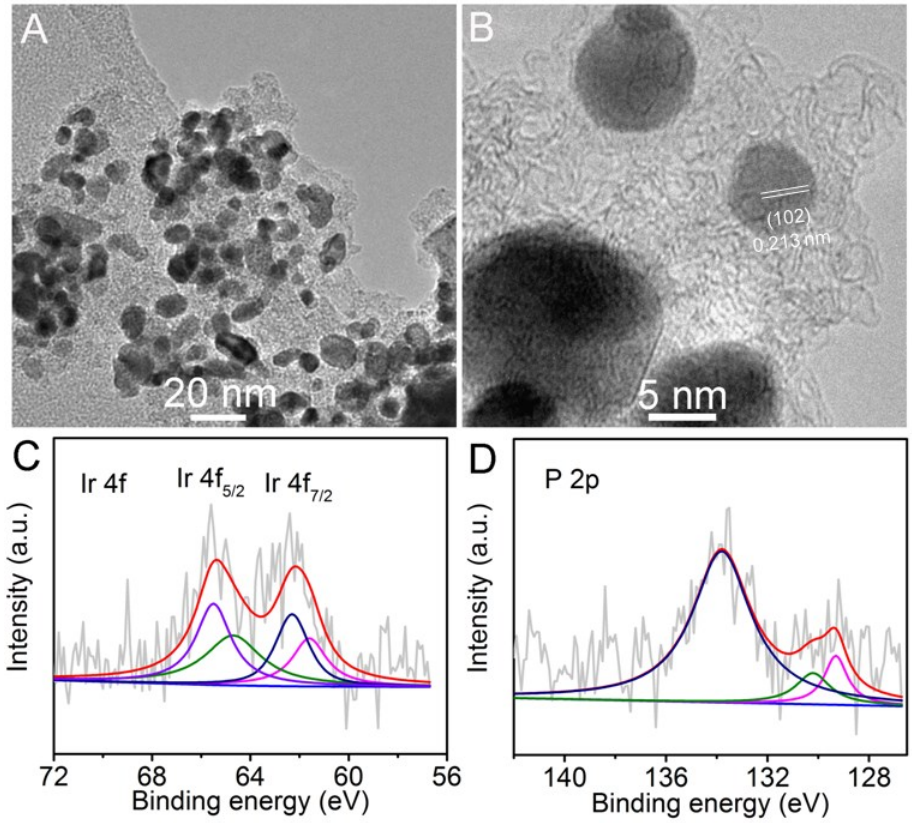

Fig. S11. (A) TEM and (B) HRTEM images of IrP_2@NC after electrochemical test. (C and D) The high-resolution XPS spectra of the IrP_2@NC.

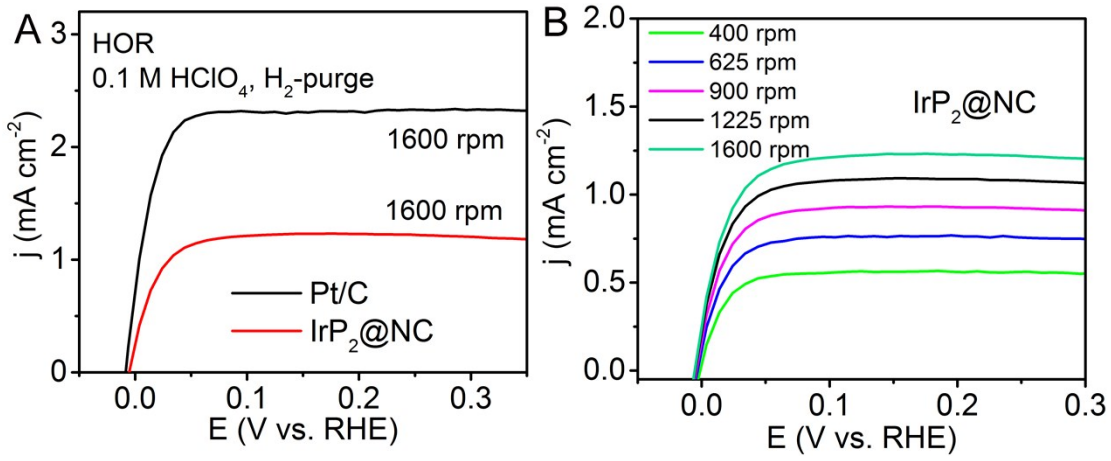

Fig. S12. (A) Polarization curves of IrP_2@NC, and Pt/C for HOR in H_2-saturated 0.1 M $HClO_4$. (B) HOR polarization curves on IrP_2@NC catalyst at different rotation rates from 400 to 1600 rpm.

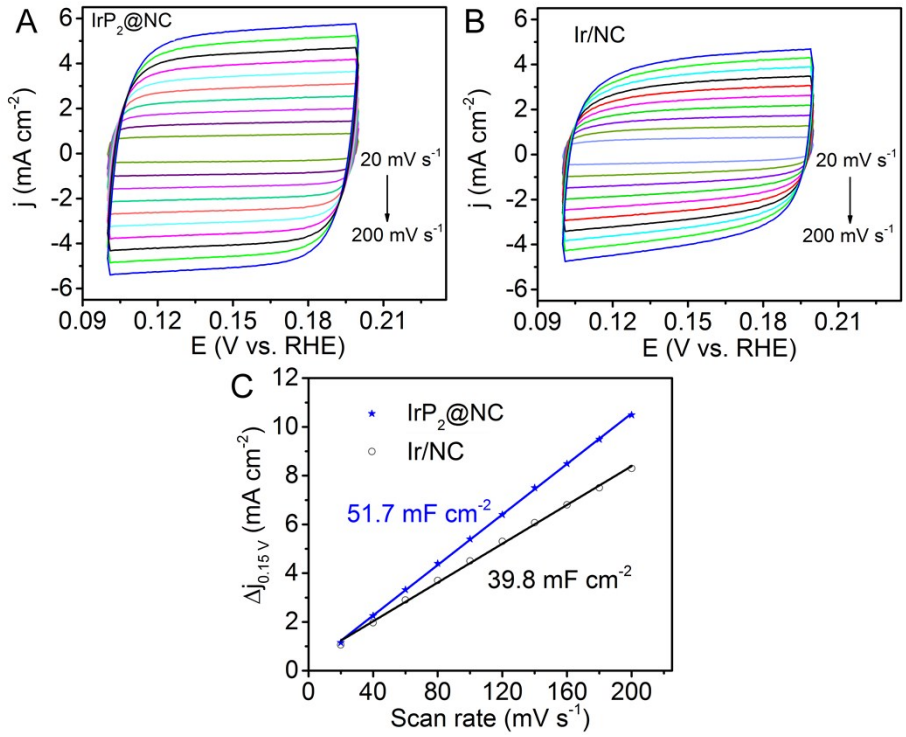

Fig. S13. CVs for (A) IrP_2/NC, (B) Ir/NC, (C) The difference in current density (j) between the anodic and cathodic sweeps ($\triangle j = j_a - j_c$) versus scan rate; the slope of the fitting line is used for determination of the double-layer capacitance (C_{dl}).

Electrochemical active surface area (ECSA): The electrochemical active surface area (ECSA) of the catalyst was estimated from the double-layer capacitance (C_{dl}). Therefore, the electrochemical capacitance was evaluated via cyclic voltammetry in the potential range of 0.10– 0.20 V versus RHE. Each CV segment was swept three times at each scan rate (20, 40, 60, 80, 100, 120, 140, 160, 180 and 200 mV s^{-1}) before recording the CV curves shown in Figure S13, inset). The capacitive currents were then analyzed at the potential of 0.15 V versus RHE, and plotted as a function of the scan rate (**Fig. S12**). The slope of the linear fit yields the specific capacitance of ~51.7 and 39.8 mF cm^{-2} for IrP_2/NC and Ir/NC.

By considering the specific capacitance of an atomically smooth planar surface with a real surface area of 1.0 cm^2 and specific capacitance (C_s) generally within 20–60 μF cm^{-2} range alkaline media,[7-9] the specific capacitance can be translated into the ECSA by calculation from the following equation. Herein, by using the midpoint specific capacitance of 40 μF cm^{-2}, the ECSA of rP_2/NC is determined as:

$ECSA = C_{dl}/C_s$ = 51.7 mF cm^{-2}/40 μF cm^{-2} per cm^2_{ECSA} = ~1292 cm^2

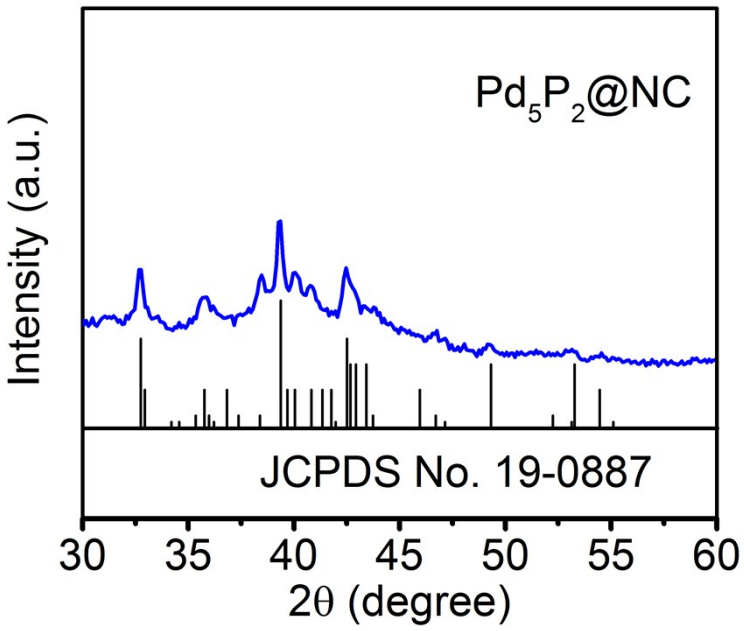

Fig. S14. XRD pattern of Pd_5P_2@NC.

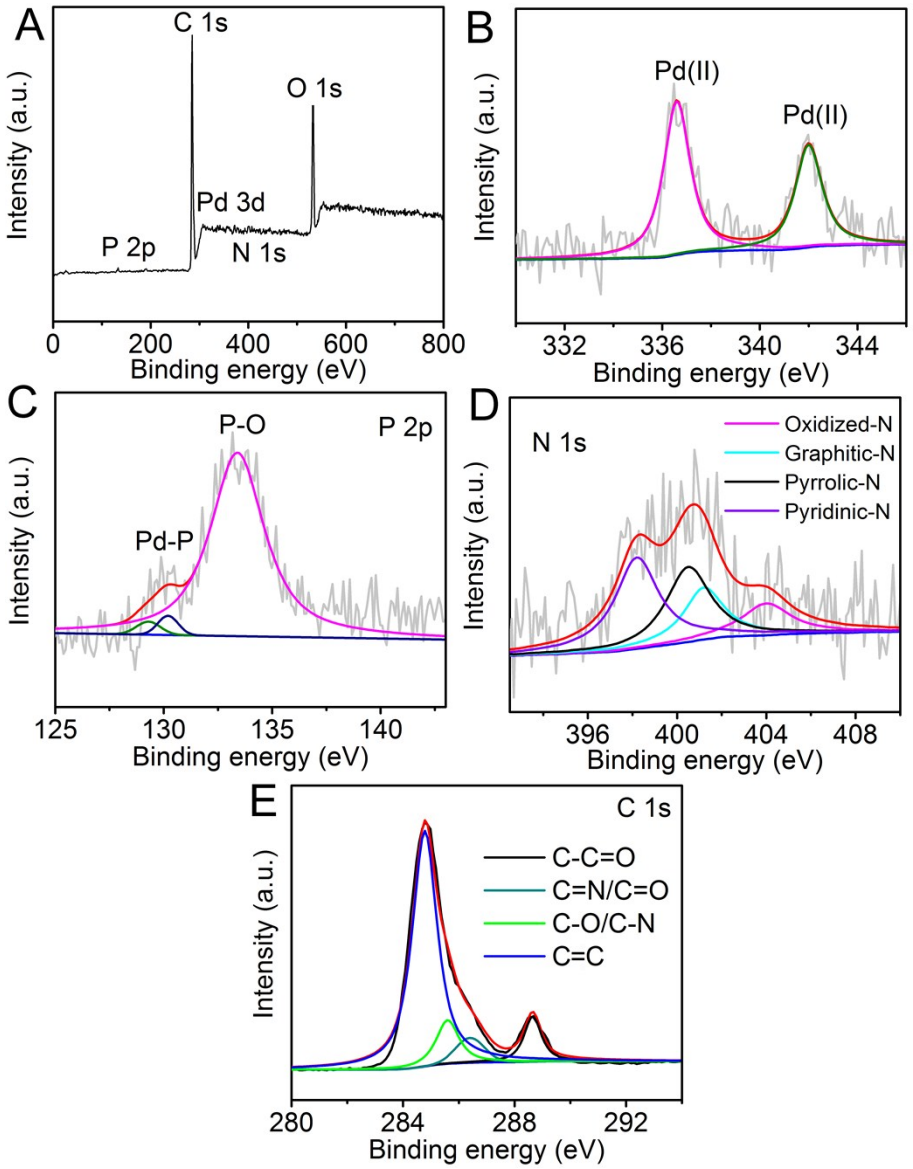

Fig. S15. (A) XPS survey pattern of Pd_5P_2@NC. (B-E) The high-resolution XPS spectra of the Pd_5P_2@NC.

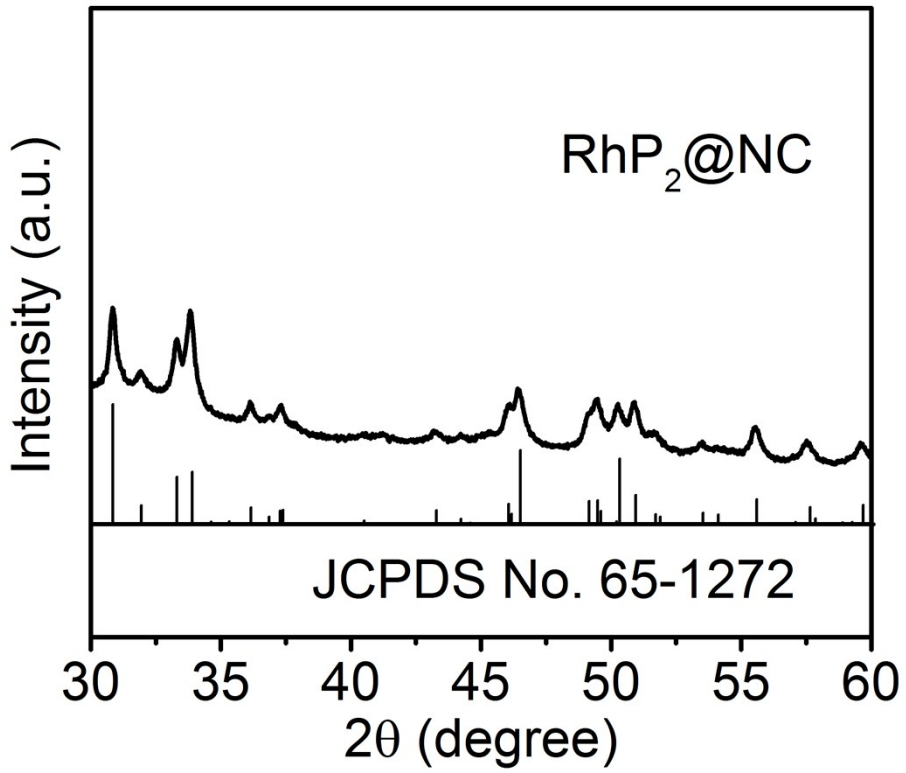

Fig. S16. XRD pattern of RhP_2@NC.

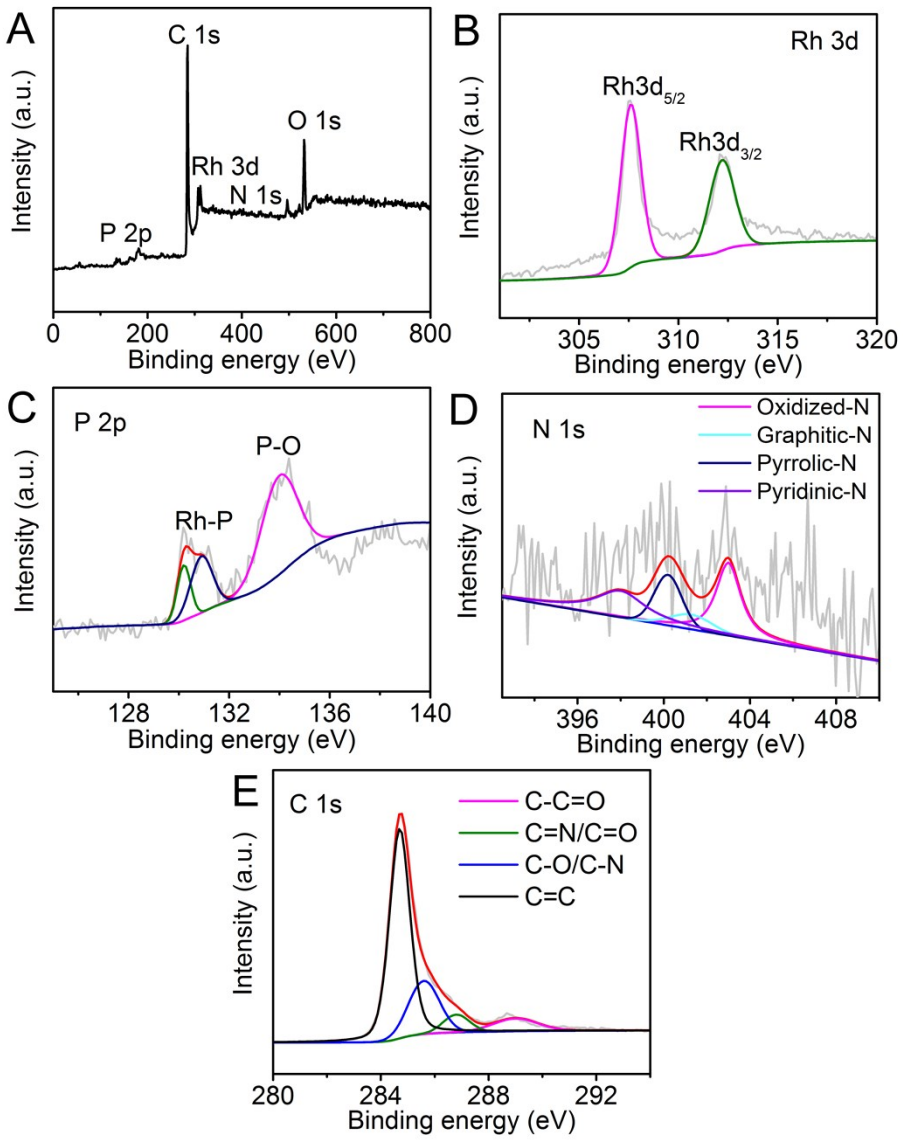

Fig. S17. (A) XPS survey pattern of RhP_2@NC. (B-E) The high-resolution XPS spectra of the RhP_2@NC.

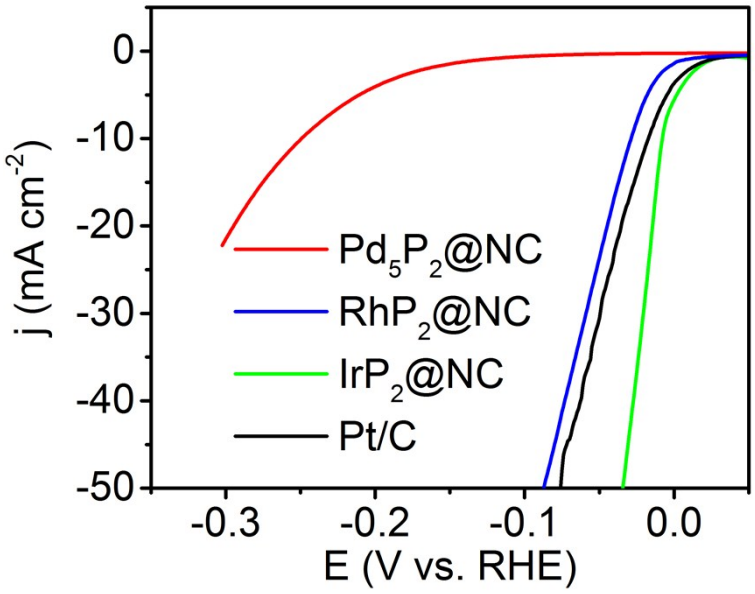

Fig. S18. HER polarization curves for Pd_5P_2@NC, RhP_2@NC, IrP_2@NC and Pt/C recorded at 5 mV s^{-1}.

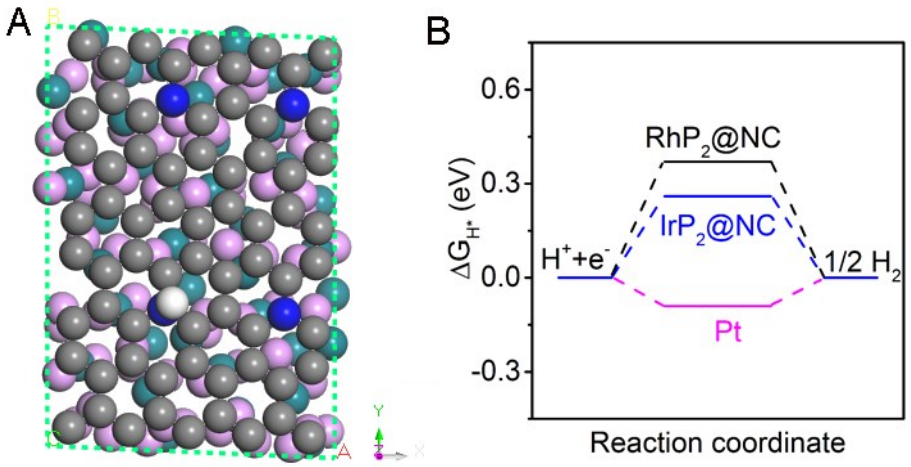

Fig. S19. (A) Theoretical models used in DFT calculation, and adopted adsorption sites of H* on the surface of the RhP_2@NC model. (B) Calculated free-energy diagram of HER at equilibrium potential for RhP_2@NC, IrP_2@NC and Pt.

Table S1 Comparison of HER performance in acid and alkaline media for IrP_2@NC with other HER electrocatalysts.

Catalysts	Electrolytes/(pH)	Overpotential@j ($mV@mA\ cm^{-2}$)	Tafel slope ($mV\ dec^{-1}$)	Catalyst loading ($mg\ cm^{-2}$)	Ref.
IrP_2@NC	0.5 M H_2SO_4	8@10	28	0.7	This work
	1.0 M KOH	28@10	50		
CoP/CC	0.5 M H_2SO_4	67@10	51	0.92	10
	1.0 M KOH	209@10	129		
np-CoP NWs/Ti	0.5 M H_2SO_4	95@20	65	0.8	11
	1.0 M KOH	150@20	71		
CoP@BCN	0.5 M H_2SO_4	87@10	46	0.4	12
	1.0 M KOH	215@10	52		
WP NAs/CC	0.5 M H_2SO_4	130@10	69	2.0	13
	1.0 M KOH	150@10	102		
WP_2 SMPs	0.5 M H_2SO_4	161@10	57	0.5	14
	1.0 M KOH	153@10	60		
WP_2 NRs	0.5 M H_2SO_4	347@10	52	-	15
	1.0 M KOH	225@10	84		
WP_2 NPs/W	0.5 M H_2SO_4	143@10	66	0.2	16
	1.0 M KOH	214@10	92		
WP NPs@NC	0.5 M H_2SO_4	102@10	58	2.0	17
	1.0 M KOH	150@10			
MoP_2 NS/CC	0.5 M H_2SO_4	58@10	63.6	0.8	18
	1.0 M KOH	85@10	70.0		
MoP NA/CC	0.5 M H_2SO_4	124@10	58	2.5	19
	1.0 M KOH	80@10	83		
MoP_2 NPs/Mo	0.5 M H_2SO_4	143@10	57	-	20
	1.0 M KOH	194@10	80		
MoP NPs@NC	0.5 M H_2SO_4	115@10	65	2.0	21

	1.0 M KOH	80@10	59		
FeP NPs@NPC	0.5 M H_2SO_4	130@10	67	1.4	22
	1.0 M KOH	214@10	82		
Mn-CoP/Ti	0.5 M H_2SO_4	49@10	55	5.61	23
	1.0 M KOH	76@10	52		
$NiCo_2P_x$/CF	0.5 M H_2SO_4	104@10	59.6	5.9	24
	1.0 M KOH	58@10	34.3		
np-$(Co_{052}Fe_{0.48})_2P$	0.5 M H_2SO_4	64@10	45	2.5	25
	1.0 M KOH	79@10	40		
Ni_2P/Ti	0.5 M H_2SO_4	130@20	46	1.0	26
Ni_2P	0.5 M H_2SO_4	140@20	66	0.38	27
	1.0 M KOH	250@20	102		
NiP_2 NS/CC	0.5 M H_2SO_4	75@10	51	4.3	28
	1.0 M KOH	102@10	65		
CoP/CNT	0.5 M H_2SO_4	122@10	54	0.285	29
CoP/Ti	0.5 M H_2SO_4	85@20	50	2.0	30
Co-P/Cu foil	1.0 M NaOH	94@10	42	-	31
FeP	0.5 M H_2SO_4	50@10	37	1.0	32
MoP	0.5 M H_2SO_4	180@30	54	0.86	33
Mo_2C@NC	0.5 M H_2SO_4	124@10	-	0.28	34
	1.0 M KOH	60@10	-		
15-h-CoS_2	0.5 M H_2SO_4	200@12.37	72	-	35
	1.0 M KOH	244@10	133		
Co-NCNT/CC	0.5 M H_2SO_4	78@10	74	3.4	36
	1.0 M KOH	180@10	193		
CoNC/GD	0.5 M H_2SO_4	340@10	138	-	37
	1.0 M KOH	284@10	115		
WN NA/CC	0.5 M H_2SO_4	198@10	62	2.5	38
	1.0 M KOH	285@10	170		
WON@NC NAs/CC	0.5 M H_2SO_4	106@10	65	7.7	39

	1.0 M KOH	130@10	128		
Mo_2C QD/NGCL	0.5 M H_2SO_4	136@10	68.4	1.0	40
	1.0 M KOH	111@10	57.8		
P-W_2C@NC	0.5 M H_2SO_4	89@10	53	3.5	41
	1.0 M KOH	63@10			
1D-RuO_2-CN_x	0.5 M H_2SO_4	93@10	40	~0.17	42
	0.5 M KOH	95@10	70		
Co-Ni-B	0.1 M $HClO_4$	209@10	-	2.1	43
	1.0 M NaOH	133@10	-		
$Zn_{0.3}Co_{2.7}S_4$	0.5 M H_2SO_4	80@10	47.5	0.285	44
	1.0 M KOH	85@10			
CNF@CoS_2	0.5 M H_2SO_4	110@10	66.8	6.6	45
	1.0 M KOH	207@10	113.3		
Ni-C-N NSs	0.5 M H_2SO_4	60.9@10	32	0.2	46
	1.0 M KOH	30.8@10	-		
Co-C-N	0.5 M H_2SO_4	138@10	55	-	47
	1.0 M KOH	178@10	102		
Co-NRCNTs	0.5 M H_2SO_4	260@10	80	0.28	48
	1.0 M KOH	370@10	-		
Co-Mo-S_x	0.1 M $HClO_4$	~250@5	-	0.05	49
	0.1 M KOH	~201@5	-		
NiAu/Au	0.5 M H_2SO_4	~50@10	36	-	50
Ru/C_3N_4/C	0.5 M H_2SO_4	~75@10	-	-	51
	0.1 M KOH	79@10			
Ru/GO	0.5 M H_2SO_4	53@10	30		52
	1.0 M KOH	8@10	44		
Ru/Co	1.0 M KOH	28@10	31	0.275	53
Ru@C_2N	0.5 M H_2SO_4	22@10	30		54
Rh_2P	0.5 M H_2SO_4	5.4@5		3.7μgRh cm^{-2}	55
Rh/Si	0.5 M H_2SO_4	110@50			56

Pt_3Ni_2-NWs	1.0 M KOH	42@10	-	0.015	57
IrNi NCs	0.5 M H_2SO_4	32@20		12.5 μgIr cm^{-2}	58
IrCo-PHNC	0.1 $HClO_4$	21@10		10.0μgIr cm^{-2}	59

References

1 G. Kresse and J. Hafner, *Phys. Rev. B,* **1993**, *47*, 558–561.
2 G. Kresse and J. Hafner, *Phys. Rev. B,* **1994**, *49*, 14251–14269.
3 P. E. Blochl, *Phys. Rev. B,* **1994**, *50*, 17953–17979.
4 G. Kresse and D. Joubert, *Phys. Rev. B,* **1999**, *59*, 1758–1775.
5 S. J. Grimme, *Comput. Chem.,* **2006**, *27*, 1787–1799.
6 Z. Kou, X. Kai, Z. Pu and S. Mu, *Nano Energy,* **2017**, *36*, 374–380.
7 J. Kibsgaard and T. F. Jaramillo. *Angew. Chem. Int. Ed.* 2014, **53**, 14433-14437.
8 C. C. L. McCrory, S. Jung, J. C. Peters and T. F. Jaramillo. *J. Am. Chem. Soc.* 2013, **135**, 16977-16987.
9 G. Wu, N. Li, D. R. Zhou, K. Mitsuo and B. Q. Xu. *J. Solid State Chem.* 2004, **177**, 3682-3692.
10 J. Tian, Q. Liu, A. M. Asiri and X. Sun, *J. Am. Chem. Soc.,* **2014**, *136*, 7587–7590.
11 S. Gu, H. Du, A. M. Asiri, X. Sun and C. Li, *Phys. Chem. Chem. Phys*., **2014**, *16*, 16909–16913.
12 H. Tabassum, W. Guo, W. Meng, A. Mahmood, R. Zhao, Q. Wang and R. Zou, *Adv. Energy Mater.,* DOI: 10.1002/aenm.201601671.
13 Z. Pu, Q. Liu, A. M. Asiri, and X. Sun, *ACS Appl Mater Interfaces,* **2014**, *6*, 21874–21879.
14 Z. Xing, Q. Liu, A. M. Asiri and X. Sun, *ACS Catal.,* **2015**, *5* 145–149.
15 H. Du, S. Gu, R. Liu and C. Li, *J. Power Sources,* **2015**, *278*, 540–545.
16 Z. Pu, I. S. Amiinu and S. Mu, *Energy Technol.,* **2016**, *4*, 1030–1034.
17 Z. Pu, X. Ya, I. S. Amiinu, Z. Tu, X. Liu, W. Li and S. Mu, *J. Mater. Chem. A,* **2016**, *4*, 15327–15332.
18 W. Zhu, C. Tang, D. Liu, J. Wang, A. M. Asiri and X. Sun, *J. Mater. Chem. A,* **2016**, *4*, 7169–7173.
19 Z. Pu, S. Wei, Z. Chen and S. Mu, *Appl. Catal. B: Environ.,* **2016**, *196,* 193–198.
20 Z. Pu, I. S. Amiinu, M. Wang, Y. Yang and S. Mu, *Nanoscale* **2016**, *8*, 8500–8504.
21 Z. Pu, I. S. Amiinu, X. Liu, M. Wang, S. Mu, *Nanoscale,* **2016**, *8*, 17256–17261.
22 Z. Pu, Y. Xue, I. S. Amiinu, C. Zhang, M. Wang, Z. Kou and S. Mu, *Nanoscale,* **2017**, *9*, 3555–3560.
23 T. Liu, X. Ma, D. Liu, S. Hao, G. Du, Y. Ma, A. M. Asiri, X. Sun and L. Chen, *ACS Catal.,* **2017**, *7*, 98–102.
24 R. Zhang, X. Wang, S. Yu, T. Wen, X. Zhu, F. Yang, X. Sun, X. Wang and W. Hu, *Adv. Mater.,* **2017**, *29*, 1605502.
25 Y. Tan, H. Wang, P. Liu, Y. Shen, C. Cheng, A. Hirata, T. Fujita, Z. Tang and M. Chen, *Energy Environ. Sci,*. **2016**, *9*, 2257–2261.
26 E. J. Popczun, J. R. McKone, C. G. Read, A. J. Biacchi, A. M. Wiltrout, N. S. Lewis and R. E. Schaak, *J. Am. Chem. Soc.,* **2013**, *135*, 9267–9270.

27 L. Feng, H. Vrubel, M. Bensimon and X. Hu, *Phys. Chem. Chem. Phys.,* **2014**, *16*, 5917–5921.
28 P. Jiang, Q. Liu and X. Sun, *Nanoscale,* **2014**, *6*, 13440–13445.
29 Q. Liu, J. Tian, W. Cui, P. Jiang, N. Cheng, A. M. Asiri and X. Sun, *Angew. Chem., Int. Ed.,* **2014**, *53*, 6710–6714.
30 E. J. Popczun, C. G. Read, C. W. Roske, N. S. Lewis and R. E. Schaak, *Angew. Chem., Int. Ed.,* **2014**, *126*, 5531–5534.
31 N. Jiang, B. You, M. Sheng and Y. Sun, *Angew. Chem., Int. Ed.,* **2015**, *54*, 6251–6254.
32 F. Juan, J. Callejas, M. McEnaney, C. G. Read, J. C. Crompton, A. J. Biacchi, E. J. Popczun, T. R. Gordon, N. S. Lewis and R. E. Schaak, *ACS Nano,* **2014**, *8*, 11101–11107.
33 P. Xiao, M. A. Sk, L. Thia, X. Ge, R. J. Lim, J. Y. Wang, K. H. Lim and X. Wang, *Energy Environ. Sci.,* **2014**, *7*, 2624–2629.
34 X. Zou, X. Huang, A. Goswami, R. Silva, B. R. Sathe, E. Mikmekova, T. Asefa, *Angew. Chem., Int. Ed.* **2014**, *126*, 4372–4376.
35 H. Zhang, Y. Li, G. Zhang, P. Wan, T. Xu, X. Wu and X. Sun, *Electrochimi. Acta,* **2014**, *148*, 170–174.
36 Z. Xing, Q. Liu, W. Xing, A. M. Asiri and X. Sun, *ChemSusChem,* **2015**, *8*, 1850–1855.
37 Y. Xue, J. Li, Z. Xue, Y. Li, H. Liu, D. Li, W. Yang and Y. Li, *ACS Appl. Mater. Interfaces,* **2016**, *8*, 31083−31091.
38 J. Shi, Z. Pu, Q. Liu, A. M. Asiri, J. Hu and X. Sun, *Electrochimi. Acta,* **2015**, *154*, 345–351.
39 Q. Li, W. Cui, J. Tian, Z. Xing, Q. Liu, W. Xing, A. M. Asiri and X. Sun, *ChemSusChem,* **2015**, *8*, 2487–2491.
40 Z. Pu, M. Wang, Z. Kou, I. S. Amiinu and S. Mu, *Chem. Commun.,* **2016**, *52*, 12753–12756.
41 G. Yan, C. Wu, H. Tan, X. Feng, L. Yan, H. Zang and Y. Li, *J. Mater. Chem. A,* **2017**, *5*, 765–772.
42 T. Bhowmik, M. Kundu and S. Barman, *ACS Appl. Mater. Interfaces,* **2016**, *8*, 28678−28688.
43 S. Gupta, N. Patela, R. Fernandes, R. Kadrekar, A. Dashora, A. K. Yadav, D. Bhattacharyya, S. N. Jha, A. Miotello and D. C. Kothari, *Appl. Catal. B: Environ*., **2016**, *192*, 126–133.
44 Z. Huang, J. Song, K. Li, M. Tahir, Y. Wang, L. Pan, L. Wang, X. Zhang and J. Zou, *J. Am. Chem. Soc.,* **2016**, *138*, 1359–1365.
45 H. Gu, Y. Huang, L. Zuo, W. Fan and T. Liu, *Inorg. Chem. Front.,* **2016**, *3*, 1280–1288.
46 J. Yin, Q. Fan, Y. Li, F. Cheng, P. Zhou, P. Xi and S. Sun, *J. Am. Chem. Soc.,* **2016**, *138*, 14546–14549.
47 S. Wang, X. Hao, Z. Jiang, X. Sun, D. Xu, J. Wang, H. Zhong, F. Meng and X. Zhang, *J. Am. Chem. Soc.,* **2015**, *137*, 15070–15073.
48 X. Zou, X. Huang, A. Goswami, R. Silva, B. R. Sathe, E. Mikmekova and T.

Asefa, *Angew. Chem., Int. Ed.,* **2014**, *126*, 4461–4465.
49 J. S. Jirkovský, C. D. Malliakas, P. P. Lopes, N. Danilovic, S. S. Kota, K. C. Chang, B. Genorio, D. Strmcnik, V. R. Stamenkovic, M. G. Kanatzidis and N. M. Markovic, *Nat. Mater.,* **2016**, *15*, 197–203.
50 H. Lv, Z. Xi, Z. Chen, S. Guo, Y. Yu, W. Zhu, Q. Li, X. Zhang, M. Pan, G. Lu, S. Mu and S. Sun, *J. Am. Chem. Soc.,* **2015**, *137*, 5859–5862.
51 Y. Zheng, Y. Jiao, Y. Zhu, L. Li, Y. Han, Y. Chen, M. Jaroniec and S. Qiao, *J. Am. Chem. Soc.,* **2016**, *138*, 16174–16181.
52 R. Ye, Y. Liu, Z. Peng, T. Wang, A. S. Jalilov, B. I. Yakobson, S. Wei and J. M. Tour, *ACS Appl. Mater. Interfaces,* **2017**, *9*, 3785−3791.
53 J. Su, Y. Yang, G. Xia, J. Chen, P. Jiang and Q. Chen, *Nat. Commun.,* **2017**, *8*, 14969.
54 J. Mahmood, F. Li, S. Jung, M. S. Okyay, I. Ahmad, S. J. Kim, N. Park, H. Y. Jeong and J. B. Baek, *Nat. Nanotechnol.,* **2017**, *12*, 441–446.
55 F. Yang, Y. Zhao, Y. Du, Y. Chen, G. Cheng, S. Chen and W. Luo, *Adv. Energy Mater.,* **2018,** *8***,** 1703489.
56 L. Zhu, H. Lin, Y. Li, F. Liao, Y. Lifshitz, M. Sheng, S. T. Lee and M. Shao, *Nat. Commun.,* **2016**, *7*, 12272.
57 P. Wang, X. Zhang, J. Zhang, S. Wan, S. Guo, G. Lu, J. Yao and X. Huang, *Nat. Commun.,* **2017**, *8*, 14580.
58 Y. Pi, Q. Shao, P. Wang, J. Guo and X. Huang, *Adv. Funct. Mater.,* **2017**, *27*, 1700886.
59 J. Feng, F. Lv, W. Zhang, P. Li, K. Wang, C. Yang, B. Wang, Y. Yang, J. Zhou, F. Lin, G. Wang and S. Guo, *Adv. Mater.,* **2017**, *29*, 21703798.